BBA - Bioenergetics 1860 (2019) 147–154

Contents lists available at ScienceDirect

BBA - Bioenergetics

journal homepage: www.elsevier.com/locate/bbabio

Efficiency of excitation energy trapping in the green photosynthetic bacterium *Chlorobaculum tepidum*

Reza Ranjbar Choubeh[a], Rob B.M. Koehorst[a,d], David Bína[e], Paul C. Struik[b], Jakub Pšenčík[c], Herbert van Amerongen[a,d,*]

[a] Laboratory of Biophysics, Wageningen University, Wageningen, the Netherlands
[b] Centre for Crop Systems Analysis, Wageningen University, Wageningen, the Netherlands
[c] Department of Chemical Physics and Optics, Faculty of Mathematics and Physics, Charles University, Prague, Czech Republic
[d] MicroSpectroscopy Research Facility, Wageningen University, Wageningen, the Netherlands
[e] Faculty of Science, University of South Bohemia, České Budějovice, Czech Republic

A B S T R A C T

During the millions of years of evolution, photosynthetic organisms have adapted to almost all terrestrial and aquatic habitats, although some environments are obviously more suitable for photosynthesis than others. Photosynthetic organisms living in low-light conditions require on the one hand a large light-harvesting apparatus to absorb as many photons as possible. On the other hand, the excitation trapping time scales with the size of the light-harvesting system, and the longer the distance over which the formed excitations have to be transferred, the larger the probability to lose excitations. Therefore a compromise between photon capture efficiency and excitation trapping efficiency needs to be found. Here we report results on the whole cells of the green sulfur bacterium *Chlorobaculum tepidum*. Its efficiency of excitation energy transfer and charge separation enables the organism to live in environments with very low illumination. Using fluorescence measurements with picosecond resolution, we estimate that despite a rather large size and complex composition of its light-harvesting apparatus, the quantum efficiency of its photochemistry is around ~87% at 20 °C, ~83% at 45 °C, and about ~81% at 77 K when part of the excitation energy is trapped by low-energy bacteriochlorophyll *a* molecules. The data are evaluated using target analysis, which provides further insight into the functional organization of the low-light adapted photosynthetic apparatus.

1. Introduction

Photosynthesis provides energy for the majority of organisms on Earth. The process starts in light-harvesting (LH) complexes, which absorb light and transfer the excitation energy to reaction centers (RCs). In these RCs, charge separation (CS) occurs, which drives chemical reactions that ultimately result in storage of light energy in a chemical form. While all RCs are structurally similar, the need to adapt to different light conditions has led to the evolution of a broad diversity of LH complexes [3,8,22]. Both the overall composition and spatial organization of the photosynthetic apparatus play an important role in tuning the photosynthetic performance. A good understanding of the principles allowing photosynthetic organisms to live phototrophically at very different light conditions may help in our search for new ways to capture and utilize solar energy. The efficiency of solar cells, for instance, often declines with decreasing irradiance [36]. In this respect, green sulfur bacteria are an excellent source of inspiration. Some of them are able to live at extremely low light intensities using photosynthesis as their sole source of energy [27] and one species of green sulfur bacteria was found to live phototrophically using the dim radiation of black smokers at the bottom of the Pacific Ocean where no sunlight penetrates [1]. The main LH complex of green sulfur bacteria is a chlorosome, a large antenna with a unique structural organization of pigments. The core of the chlorosome contains tens to hundreds of thousands of bacteriochlorophyll (BChl) molecules arranged in self-assembling aggregates [19,29,30,33]. In all other known LH complexes pigment-binding proteins determine the positions and orientations of only tens to hundreds of pigments. The aggregation of pigments in the chlorosome leads to strong excitonic coupling between the pigments, accompanied by the formation of charge-transfer states [17] and is responsible for the light-harvesting and energy-transferring properties of the chlorosomes. However, the substantial disorder present in chlorosomes confines the strong coupling to relatively small domains, which are only weakly interacting [10]. *Chlorobaculum (C.) tepidum* is a model organism for this group of green sulfur bacteria and its chlorosome dimensions are typically 200 nm × 50 nm × 20 nm [29], which makes chlorosomes the largest known photosynthetic antennas. The size of the chlorosome together with the very high pigment concentration is apparently essential for efficient photon gathering at low-light conditions. However, efficient energy transfer of the formed

* Corresponding author at: Laboratory of Biophysics, Wageningen University, Wageningen, the Netherlands.
E-mail address: herbert.vanamerongen@wur.nl (H. van Amerongen).

https://doi.org/10.1016/j.bbabio.2018.12.004
Received 11 October 2018; Received in revised form 7 December 2018; Accepted 8 December 2018
Available online 08 December 2018

excitations to the RCs is also crucial and that is why the overall arrangement of the photosynthetic apparatus is important [8,29,35]. Green sulfur bacteria exhibit an unusual organization of their intermediate LH complexes. In contrast to higher plants, most of these LH complexes are peripheral, meaning that they are located outside the photosynthetic membrane [4,35]. Excitations created in the chlorosome interior are transferred to the BChl *a* molecules in the baseplate of the chlorosome, which is a paracrystalline array of CsmA/BChl *a* pigment-protein complexes, together called the baseplate. A detailed structure of the baseplate is not available but several models have been proposed [28,32]. The baseplate makes contact with the BChl-*a*-containing Fenna–Matthews–Olson (FMO) antenna complexes, which in turn are attached to the cytoplasmic membrane. Excitations are thought to travel from the chlorosome interior, via the baseplate and the FMO complexes to the RCs located in the cytoplasmic membrane. The structure of the FMO complex is known [2,14,24,46] and the closely packed BChl *a* molecules allow ultrafast EET through the FMO complex [13,26,42,49]. The RC contains its own core antenna, which constitutes the only LH complex of green sulfur bacteria embedded in a membrane. The FMO complex and core antenna of the RC contain BChl *a* as the only chlorophyll-like pigment and together with the baseplate they exhibit highly overlapping spectra [12].

For the description of the effectiveness of photosynthesis, the quantum efficiency of photochemistry plays an important role. It covers all the processes from the photon absorption in light-harvesting complexes up to the charge separation in the reaction centers. The quantum efficiency of photochemistry in green sulfur bacteria is a matter of debate. Values close to 100% would be expected for low-light adapted organisms, as found for distantly related photosystem I or some photosynthetic bacteria [23,37,53]. On the other hand, the larger complexity of the photosynthetic apparatus of green sulfur bacteria, together with its extremely large size might lead to losses. In the literature ultrafast EET in the chlorosomes has been reported [15,39,41]. Fluorescence excitation spectra revealed that the efficiency of energy transfer from BChl *c* to BChl *a* in whole cells of green sulfur bacteria is close to 100% at anaerobic conditions, which are natural to these bacteria [50]. However, at room temperature it is difficult to distinguish between the contributions of BChl *a* from the baseplate, the FMO complex and the core antenna, and therefore to decide whether the excitation was transferred with such a high efficiency from the chlorosome up to the RCs, or only to the baseplate or FMO complex. In measurements performed on isolated FMO-RC complexes or membranes the efficiency of energy transfer from the FMO complexes to the RCs has never been observed to be higher than 40% [20]. A recent study on isolated membranes at 77 K, however, yielded an FMO-to-RC excitation energy transfer (EET) efficiency of ~48% [25]. According to the authors, EET from BChl *c* to the RCs cannot be observed at 77 K because the excitation energy is trapped in the baseplate and does not reach FMO due to the low temperature. In another study, the use of two-dimensional coherent spectroscopy allowed to distinguish several energy transfer steps in whole cells at 77 K and a much higher transfer efficiency of 75% was estimated [11]. This suggests that the photosynthetic apparatus is vulnerable to damage during isolation and the use of whole cells is a prerequisite for obtaining realistic efficiencies. However, it was not possible to determine whether the less than 100% efficiency is a consequence of performing the experiments at low temperature, or whether it is an intrinsic property of the modular organization of the light-harvesting complexes.

Here we report results of picosecond fluorescence measurements at 20 °C and 45 °C as well as at 77 K on whole cells of *C. tepidum*. Measurements performed at 20 °C and 45 °C allow us to observe EET from BChl *c* to BChl *a* of the baseplate, FMO, and RCs at physiological relevant temperatures. The results indicate that at 20 °C (45 °C) the quantum efficiency of photochemistry is around ~87% (~83%), while the efficiency at 77 K is ~81%, which is somewhat higher than the results of Dostal et al. [11].

2. Materials & methods

2.1. Sample preparation

C. tepidum cells, grown at 45 °C, were suspended in 10–20 mM Tris-HCl buffer, pH = 8.0, and incubated with 5 mM sodium dithionite inside an air-tight quartz cuvette for at least 2 h before the time-resolved fluorescence measurements. Before and after 20 °C and 45 °C time-resolved fluorescence measurement, the absorption spectrum of the sample was recorded to check whether the sample had been exposed to oxygen, in which case the strong absorption of sodium dithionite at around 315 nm would be absent. Before performing the 77 K measurements, the absorption spectrum was also measured at room temperature.

2.2. Absorption measurements

Absorption spectra of *C. tepidum* cells were recorded on a Cary 5E spectrophotometer, equipped with an integrating diffuse reflectance sphere (DRA-CA-50, Labsphere) to correct for light scattering by the cells. The optical path length was 1 cm. All measurements were performed at room temperature.

2.3. Time-resolved fluorescence measurements

Picosecond fluorescence measurements were performed on *C. tepidum* cells at 20 °C, 45 °C, and 77 K by using a synchroscan streak-camera system as described before ([7,48]). At 20 °C, we used three time windows to record the fluorescence, namely 160 ps, 800 ps and 2000 ps while at 45 °C a time window of 2000 ps was used. At 77 K we used a time window of 800 ps and 2000 ps. At 20 °C, the instrument response function, IRF, was recorded before each measurement. The IRF was fitted with a sum of two or three Gaussian functions to describe the IRF mathematically as accurately as possible. The Full Width at Half Maximum (FWHM) of the Gaussian function with the largest contribution was 6 ps, 9 ps, 22 ps, at time windows 160 ps, 800 ps, and 2000 ps, respectively. For the 45 °C and 77 K measurements, the IRF was modeled with one Gaussian for which the FWHM was similar to what was mentioned earlier for measurements performed at 20 °C.

We used 400 nm excitation light to perform 20 °C, 45 °C and 77 K measurements. All images were corrected for the detection efficiency of the streak camera. The repetition rate of the laser was 4 MHz. For 20 °C (45 °C) and 77 K measurements, the spot size was in the order of ~40 μm and ~100 μm, respectively. At 20 °C and 45 °C (only performed with 2000 ps time window) the excitation energy per pulse for time windows 160 ps, 800 ps, and 2000 ps was 1.25 pJ, 0.25–0.5 pJ, and 0.13–0.25 pJ, respectively. At 77 K the excitation energy per pulse was 0.5–1.25 pJ. All time-resolved fluorescence measurements lasted 20–40 min. Several 20 °C measurements with varying intensity were performed to assess at which excitation energy per pulse exciton-exciton annihilation occurred (data not shown). At 2.5 pJ the lifetimes were slightly shorter indicating a small amount of exciton-exciton annihilation at this intensity.

For 20 °C (45 °C) and 77 K measurements, the optical density of the samples was 0.15–0.2 and ~0.8 at 740 nm, respectively, measured at room temperature in a quartz cuvette with 1 cm optical path length. The 20 °C (45 °C) time-resolved measurements were done using a quartz cuvette with an optical path of 1 cm. For 77 K time-resolved measurements, the samples were collected quickly from a quartz cuvette (only used to keep the cells in an anaerobic environment before the 77 K measurements) in a glass Pasteur pipette with ~1 mm diameter (which made the optical density of frozen cells around 0.10 in the maximum) and frozen using liquid nitrogen. Measurements were performed on the sample in the Pasteur pipette. The excitation light was vertically polarized and the polarizer in the detection branch was set to magic angle. For 20 °C and 45 °C time-resolved measurements a Nikon CFI Plan Apo

Lambda10X objective lens with a numerical aperture of 0.45 and focal length of ~20 mm was used. For 77 K time-resolved measurements a lens with a focal length of 7 cm was used.

2.4. Target and global analysis

Global and target analyses were performed as described in [43,44], using an in-house program written in Matlab. As part of this program, OPTI TOOLBOX [9] was used.

In order to resolve the different stages of EET from the chlorosome to the baseplate and FMO complex at 20 °C, we performed simultaneous global analysis on the time-resolved data obtained with 160 ps and 800 ps time windows.

The 20 °C measurements obtained with 2000 ps time window were analyzed together globally with three lifetimes. Then, the longest lifetime obtained from this global analysis was fixed in the global analysis of 20 °C measurements with 160 ps and 800 ps time window that were fitted together with four lifetimes. It was imposed that the decay-associated spectra (DAS) should have the same shape in all different measurements. The 45 °C measurements were performed only with a 2000 ps time windows and its analysis was similar to that of 20 °C measurements performed with 2000 ps time window.

For the global analysis of the 77 K data it was also imposed that the DAS obtained with different measurements should have the same shape. The combination of the data obtained with 800 ps and 2000 ps time-windows was fitted with four lifetimes, while the data obtained with only 2000 ps time-window was fitted with three lifetimes.

3. Results & discussion

3.1. Time-resolved fluorescence of C. tepidum cells at 20 °C and 77 K

Time-resolved fluorescence spectroscopy enables to monitor EET between BChl *c* aggregates inside the chlorosomes and BChl *a* in the baseplate, FMO complexes and the core antenna of the RC. BChls *c* constitute ~97% of the total BChl content in *C. tepidum*, the other ~3% is BChl *a*. Out of this 3%, 1% is located in the baseplate and the remaining 2% is present in the FMO complexes and RC cores [18,35].

Global analysis of time-resolved fluorescence data provides a model-independent insight into EET in intact cells. Fig. 1A–B and C show the results of global analysis of the 20 °C and 77 K time-resolved fluorescence data, respectively (see SI for the global analysis of fluorescence data obtained at 45 °C). All the DAS in Fig. 1A and C are normalized to the maximum of their time-zero spectrum. The time-zero spectrum is the summation of all DAS obtained from the analysis of one sample. This spectrum is close to the fluorescence spectrum directly after excitation and relaxation to the Q_y states, provided that no additional relaxation processes occur.

All the DAS in Fig. 1B, taken from Fig. 1A, are normalized to their maxima for a better comparison of the spectral shape.

Since BChl *c* represents the vast majority of all chlorophylls in the chlorosomes, the 400 nm laser pulses mainly excite BChl *c* and to a lesser extent BChl *a*. Initially, the emission is therefore almost exclusively due to BChl *c*. Then, the excitation energy migrates from the BChl *c* molecules in the chlorosome interior to the BChl *a* molecules in the baseplate, the FMO complex and the core antenna of the RCs, which leads to a rise of fluorescence at 800–840 nm after tens of picoseconds. In the experiments we performed, the fluorescence of BChl *a* in the baseplate could not be separated from the fluorescence of BChl *a* in the FMO complex and the cores of RCs. This is in agreement with the observation that the distributions of energy levels in all these three LH complexes are highly overlapping [12], despite the fact that the fluorescence maxima for baseplate, FMO complex, and RC core differ: ~810, ~825 and ~835 nm respectively [16,21,31,34].

As a consequence, from the DAS obtained by global analysis, only energy transfer from BChl *c* to BChl *a* can be resolved, which manifests

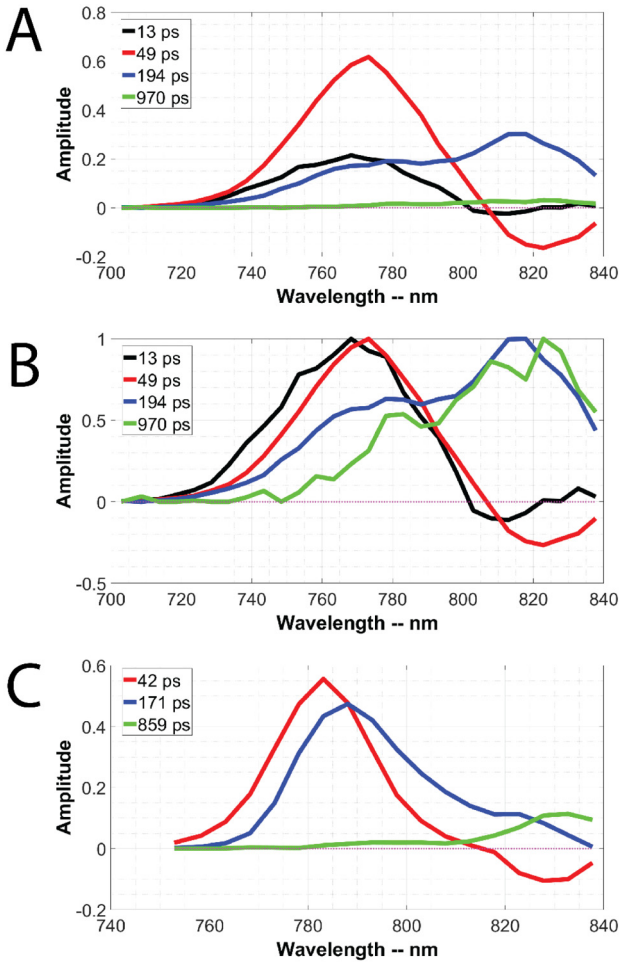

Fig. 1. A) Decay-associated spectra (DAS) obtained by global analysis of 20 °C time-resolved fluorescence measurements on *C. tepidum* cells. B) Each DAS taken from *a* is normalized to its maximum. C) DAS obtained by global analysis of 77 K time-resolved fluorescence measurements on *C. tepidum* cells. The excitation wavelength was 400 nm both at 20 °C and 77 K. All DAS in A) and C) are normalized to the maximum of the corresponding time-zero spectrum, i.e. the sum of all DAS was normalized to 1 in the maximum. The inset shows the lifetimes in ps corresponding to the DAS represented with the same color. The dotted purple line is the zero line.

itself as a positive peak at shorter wavelengths and a negative peak at longer wavelengths where BChl *c* and BChl *a* emit their fluorescence, respectively. The presence of positive and negative peaks in the same DAS, is seen in two of the 20 °C DAS in Fig. 1A and one of the 77 K DAS in Fig. 1C. Both 20 °C DAS indicate EET from BChl *c* in the chlorosome, with a positive peak at 768–773 nm, to the BChl *a* containing complexes, with negative peaks at 800–820 for the minor and 805–838 nm for the major component, and rates of $(13\,\text{ps})^{-1}$ and $(49\,\text{ps})^{-1}$, respectively. Rates of ~$(30–40\,\text{ps})^{-1}$ for EET from BChl *c* to BChl *a*, similar to the dominant $(49\,\text{ps})^{-1}$ component in the present work, were reported in other experiments performed on isolated chlorosomes [5,47]. In Fig. 1C, the 77 K DAS reflecting EET has a rate of $(42\,\text{ps})^{-1}$ with a positive peak at ~783 nm and a negative one at ~818–838 nm. This result was obtained using a 2000 ps window only and is again indicative of EET from BChl *c* to BChl *a*. Another recent study [11] on intact cells reported a somewhat slower rate of $(70\,\text{ps})^{-1}$ at 77 K for EET from BChl *c* to BChl *a* in the FMO complex. Combining the 800 ps and 2000 ps time windows a 6 ps component was observed, which indicates EET mainly between BChl *c* spectral forms and to a lesser extent EET to BChl *a* (see Fig. S1). For simplicity, we only used the 2000 ps time window data for the target analysis.

So far we looked at EET from BChl *c* to BChl *a* in the baseplate, FMO complex and the core antenna of the RC. The excitation energy is finally trapped in the RCs, and no fluorescence emission is possible anymore. The 20 °C $(194\ ps)^{-1}$ DAS (Fig. 1A–B) reflects the disappearance of excitation energy, that is "equilibrated" over all spectral species, due to trapping in the RC. It has a positive peak at ~773 nm due to BChl *c* and another positive peak at ~814 nm due to BChl *a*. At 77 K, trapping in the RCs is reflected by the $(171\ ps)^{-1}$ DAS with one positive peak at 788 nm and another positive peak at 823 nm (Fig. 1C). The peak at 823 nm reflects the excitation energy of BChl *a* that is being trapped in the RCs. Note that this component does not reflect excitations that are "equilibrated" over all spectral species since the BChl *c* peak is more pronounced than at 20 °C. This is most likely caused by EET that was slowed down at 77 K because energetic disorder (inhomogeneous broadening) in the chlorosomes leads to excitation trapping in low energy excitonic levels at low temperature (see for instance [38]). Finally, there is a very small 20 °C DAS with a decay rate of $(970\ ps)^{-1}$ (Fig. 1A–B). The $(970\ ps)^{-1}$ DAS has two positive peaks at 778–783 nm and at 800–840 nm. This DAS has a similar shape as the 20 °C $(194\ ps)^{-1}$ component (see Fig. 1B) and represents slow trapping in the RCs. Less amplitude at 778–783 nm indicates relatively lower back transfer of excitation energy to BChl *c* in comparison to the 20 °C $(194\ ps)^{-1}$ DAS. The 77 K $(859\ ps)^{-1}$ DAS (Fig. 1C) has a maximum at longer wavelengths in comparison to the 77 K $(171\ ps)^{-1}$ DAS and it reflects BChls *a,* the excitation energy of which is trapped slower (relative to the $(171\ ps)^{-1}$ DAS) in the RCs at this low temperature. The corresponding DAS at 20 °C has a very small amplitude (see Fig. 1A).

To see if EET to BChl *a* occurs faster than the time resolution of our setup we calculated the 20 °C absorption spectrum of cells from the time-zero fluorescence spectrum obtained from global analysis of 20 °C measurements applying the Kennard-Stepanov relation (See for instance [45]) (see Fig. 2). The absorption spectrum that is calculated in this way almost perfectly overlaps with the measured 20 °C absorption spectrum of the BChl *c* Q_y absorption of the chlorosomes, meaning that the excitations at "time zero" are already spectrally equilibrated over the chlorosome with a rate faster than the ~6 ps time-resolution of the streak-camera setup. It is important to note that the BChl *a* band/shoulder, which is clearly present in the measured absorption spectrum around 800 nm, is almost fully absent in the absorption spectrum that is calculated with the Kennard-Stepanov relation, which implies that EET from BChl *c* to BChl *a* occurs largely on a time scale that is slower than the ~6 ps time-resolution of the streak-camera setup (see the 13 ps and 49 ps DAS in Fig. 1A).

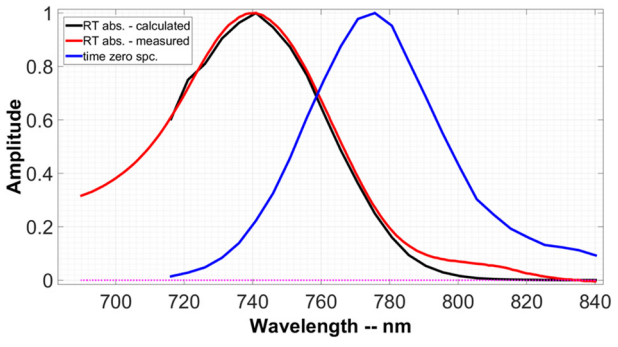

Fig. 2. The blue spectrum is the time-zero fluorescence spectrum obtained from global analysis of the time-resolved fluorescence measurements on *C. tepidum* cells at 20 °C. From this spectrum an absorption spectrum is calculated with the use of the Kennard-Stepanov relation, which is represented in black. The calculated (see text) absorption spectrum in black is compared to the measured absorption spectrum of *C. tepidum* cells at 20 °C in red. The dotted purple line is the baseline.

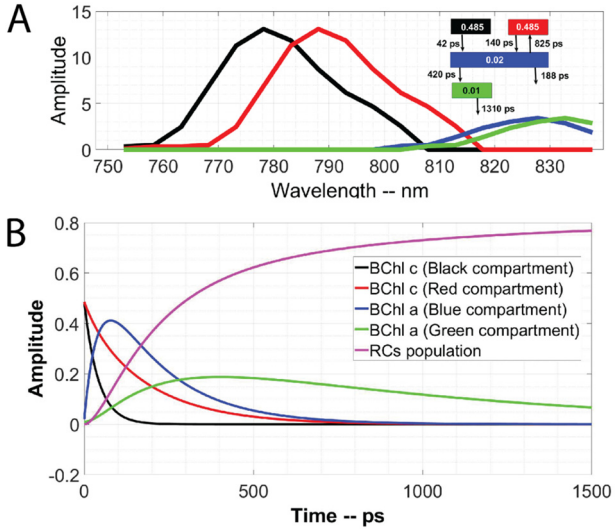

Fig. 3. A) 77 K target model and corresponding SAS of *C. tepidum*. The colors of the boxes representing the compartments are the same as for the corresponding SAS. The black and red spectra correspond to BChl *c*. The blue and green spectra correspond to BChl *a*. The initial population of each compartment is written inside the blocks representing the compartments. All compartments have a dissipative rate of $(2500\ ps)^{-1}$, which is not shown. The rates by which the blue and green compartments decay reflect trapping ($(188\ ps)^{-1}$ and $(1310\ ps)^{-1}$) in the RCs. B) The population of each compartment (same color) over time is shown. The total fraction of excitation that reach the RC is reflected by the purple curve.

3.2. Target analysis of 77 K time-resolved data of C. tepidum cells

The time-resolved fluorescence at 77 K shows a shift in the BChl *c* peak from ~784 nm to ~788 nm over a time period of ~50 ps (see Fig. S2). Thus, we need at least two compartments to represent BChl *c*. We assumed the shape of the two corresponding spectra representing BChl *c* to be the same with a separation of 10 nm relative to each other and they were forced to be zero between 810 nm and 840 nm (see Fig. 3), where BChl *c* has a much lower emission in comparison to BChl *a* (see Fig. S2). At least two spectral forms of BChl *a* exist, with decay rates of $\sim(171\ ps)^{-1}$ and $\sim(859\ ps)^{-1}$, respectively, and which are spectrally shifted by about 5 nm (see Fig. 1C). Thus, two compartments of BChl *a* were also included in the target analysis (Fig. 3). Similar as for BChl *c,* the spectra of both compartments were required to have the same shape, but they were separated by 5 nm from each other. The emission spectra of BChl *a* were forced to be zero between 750 nm and 790 nm where the emission of BChl *c* is maximum and the emission of BChl *a* is minimum (Fig. S2–S3).

We performed a target analysis simultaneously on four streak images recorded for four different samples with a 2000 ps time window. Fig. 3 shows the model used for the target analysis and the resulting rates and species associated spectra (SAS). We chose the initial population according to the relative content of BChl *c* and BChl *a* in the cells. The initial population of BChl *c* is 0.97. The best fit is obtained if this initial population is evenly distributed over the two compartments that represent BChl *c*. The initial population of BChl *a* is 0.03. There are two BChl *a* compartments; one has a lower energy than the other BChl *a* compartment. For the 77 K measurements we assumed that one third of the BChls *a* (i.e. 33% of 0.03) transfers to the RCs with a slow time constant whereas the other fraction of 0.02 corresponds to BChls *a* that transfer their excitation energy to the RCs faster. RCs are populated by the rate at which the two BChl *a* compartments decay to the ground state due to trapping (RCs are not shown in the model) and the RC population represents the trapping efficiency. For the BChl *c* and *a* compartments we set a dissipation rate of $(2500\ ps)^{-1}$ which is equal to the fluorescence lifetime of isolated BChl *a* [20]. Fig. 3B shows the

population of each compartment over time. To obtain an absolute lower bound for the efficiency, we also performed target analysis with a dissipative rate of $(859\,ps)^{-1}$ (results shown in Fig. S4), which is the longest lifetime observed in Fig. 1C.

In Fig. 3 it is shown that the energy is transferred from the black (BChl *c*) to the blue (BChl *a*) compartment with a rate of $(42\,ps)^{-1}$ which was estimated from Fig. 1C and was fixed during the fitting procedure. The obtained back transfer rate for the black compartment was extremely small and we set it to zero. The red (BChl *c*) compartment transfers its excitations to the blue compartment with a rate of $(140\,ps)^{-1}$ and the reverse process occurs with a rate of $(825\,ps)^{-1}$.

The blue compartment in Fig. 3 decays due to trapping in the RC with a rate of $(188\,ps)^{-1}$. Moreover, the blue compartment transfers its excitation energy to the green one with a rate of $(420\,ps)^{-1}$. The latter in turn decays with a rate of $(1310\,ps)^{-1}$ which was fixed during the target analysis and it represents the rate by which the excitation energy is trapped in the RCs. We chose this rate so that the total decay rate of the green compartment is $(859\,ps)^{-1}$. When the dissipative rate was $(859\,ps)^{-1}$the decay rate of the green compartment due to trapping was fixed to zero (see Fig. S4).

Assuming that both the blue and green compartments participate in trapping, with a dissipative rate of $(2500\,ps)^{-1}$ for all BChl *c* and *a* compartments, the trapping efficiency is ~80%, while only an extreme value for the dissipative rate of $(859\,ps)^{-1}$ would yield an efficiency of 45% (see Figs. 3B, S4C), which is the efficiency that was obtained for the FMO-to-RC transfer in isolated membranes [25], assuming that the dissipative rate is $(2.3\,ns)^{-1}$, therefore, it can be concluded that the efficiency of transfer is far higher in whole cells. Dostál et al. [11] estimated that 25% of the excitation energy remains trapped in the lowest energy of the FMO complexes and hence the EET efficiency from the FMO complexes to the RC is 75%. The authors stated that the exciton-exciton annihilation could have affected their estimate of this efficiency as well as trapping of the excitation energy on FMOs due to the low temperature. The excitation energy per pulse in the present study is 1000 times smaller than what was used in [11], which eliminates nearly all exciton-exciton annihilation. To avoid possible trapping of excitation energy at the baseplate (as claimed by [25]) and to obtain an efficiency of trapping which includes BChl *c* at a physiologically relevant temperature, we performed target analysis on time-resolved measurements performed on cells at 20 °C and 45 °C (see next section and Figs. S5–6 for 20 °C target analysis and Figs. S7–9 for 45 °C global and target analysis).

3.3. Target analysis of 20 °C time-resolved data of C. tepidum cells

The shape of the $(13\,ps)^{-1}$ and $(49\,ps)^{-1}$ DAS in Fig. 1A–B indicates the presence of (at least) two spectrally different compartments for BChl *c* and two for BChl *a*. Fig. 4 shows the target model used for the 20 °C time-resolved measurements together with the corresponding rates and SAS.

One possible interpretation of the two compartments for BChl *c* is that one comprises the domains of aggregates located in the vicinity of the baseplate (transfer time ~11 ps, see Fig. 4) and the other comprises the domains located in the rest of the chlorosome (transfer time 54 ps, see Fig. 4). While for the former domains it is possible to transfer excitation energy almost directly to BChl *a* in the baseplate, the excitations in the latter have to undergo a random walk throughout the large chlorosome before they get close to the baseplate. As the formation of the aggregates is based on self-assembly, there is no obvious way how to establish an energy gradient within the chlorosome. Since the majority of BChl *c* molecules is not in contact with the baseplate, this interpretation also explains why the slower component possesses a larger amplitude. Similar results were obtained for chlorosomes of BChl *e* containing *Chlorobium phaeobacteroides* [34]. The two exponential decays may also be (partly) caused by static disorder and dynamic fluctuations among the many thousands of pigment molecules in the large

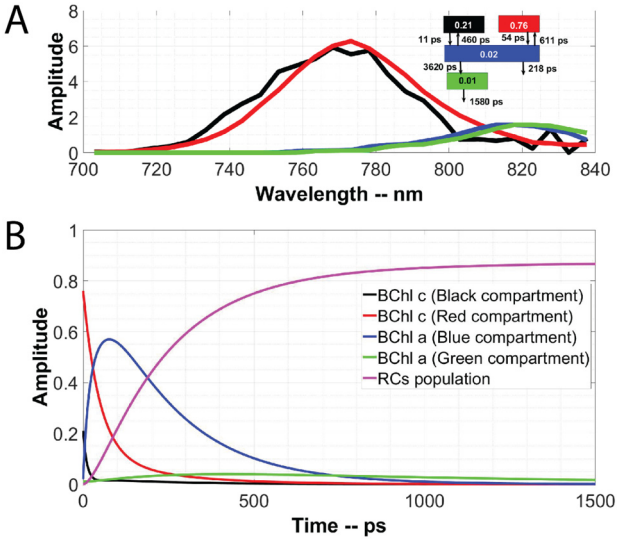

Fig. 4. A) Room temperature target model and the obtained corresponding SAS for *C. tepidum*. Each spectrum is shown with the same color as the corresponding compartment. The black and red compartments represent BChl *c*. The green and blue compartments correspond to BChl *a*. The initial fractional populations are written in the four compartments. All compartments have a dissipative rate of $(2500\,ps)^{-1}$, which is not shown. The decay rates of the blue and green compartments correspond to trapping by the RCs ($(218\,ps)^{-1}$ and $(1580\,ps)^{-1}$). B) The population of each compartment (same color) over time is shown. The total fraction of excitation that reach the RC is reflected by the purple curve.

chlorosome, which inevitably leads to a multi-exponential decay [6].

The $(970\,ps)^{-1}$ DAS (Fig. 1A–B) seems to be due to BChls *a* that temporarily "trap" the excitation energy and transfer their excitation to RCs with a slow time constant, which is far more pronounced at 77 K where less thermal energy is available. One of the BChl *a* compartments represents this group of BChl *a*. The other BChl *a* compartment represents the BChls *a* that transfer excitation energy to the RC, where trapping occurs, on a faster time scale. In the fitting, we connected the BChls *a* participating in slow trapping compartment only to the compartment of BChls *a* that participate in trapping with a faster time constant, which is somewhat arbitrary but not limiting for the conclusions drawn below. The spectral shape of the SAS representing the two BChl *a* compartments was taken to be the same with a 5 nm shift relative to each other to approximate the energy difference between the two pools, and this shift can be seen in Fig. 1B. Furthermore, the BChl *a* spectrum was set to zero between 700 nm and 750 nm, in accordance with its emission spectrum.

We chose the initial population of these compartments based on the percentages of BChl *c* and *a* in the cells. The initial population of the green compartment, representing BChl *a* with a slow trapping time, was set to 0.01. This choice does not affect the results and it could also be zero.

In Fig. 4, the black and red SAS belong to the black and red compartments, respectively, corresponding to BChl *c* in the chlorosome. The blue and green SAS in the same figure belong to the blue and green compartments, respectively, corresponding to BChl *a* of the baseplate, FMO complexes, and core antenna of the RC. The compartments of BChl *c* and *a* have a dissipative rate of $(2500\,ps)^{-1}$ similar to the value used in the analysis of the 77 K measurements. We also performed target analysis with a dissipative rate of $(970\,ps)^{-1}$ (See Fig. S5). The dissipative rate of $(970\,ps)^{-1}$ was chosen based on the longest lifetime resolved form global analysis (Fig. 1A) and represents the extreme case when the corresponding DAS indicates only dissipation instead of trapping.

The energy transfer from the black BChl *c* compartment to the blue

BChl *a* compartment in Fig. 4 is characterized by a rate of $(11\ ps)^{-1}$. The back transfer process has a rate of $(460\ ps)^{-1}$ (see SI for more details). The forward and backward EET rate between the red BChl *c* compartment and the blue BChl *a* compartment are $(54\ ps)^{-1}$ and $(611\ ps)^{-1}$, respectively.

The blue BChl *a* compartment decays largely due to charge separation in the RC with a rate of $(218\ ps)^{-1}$. In addition, the blue BChl *a* compartment transfers its excitation energy to the green BChl *a* compartment with a rate, which is on the order of several $(ns)^{-1}$. The decay rate of the green BChl *a* compartment, representing also BChls *a* that lose their excitation energy due to trapping but on a slower time scale, was fixed in the target analysis to $(1580\ ps)^{-1}$; it was chosen such that the total decay rate of the green compartment is $(970\ ps)^{-1}$ considering the dissipative rate of $(2500\ ps)^{-1}$. The blue BChl *a* compartment represents BChl *a* in the baseplate, FMO complexes, and the core antenna of the RC. The excitation energy is equilibrated over the BChls *a* in all complexes due to their large spectral overlap [12]. For the same reason also the trap states from the green BChl *a* compartment may be found in all three complexes. Most probably, these traps represent the lowest energy states of the various BChl *a* containing complexes, which are quickly populated. Energy transfer from these traps towards the RC probably requires thermal energy and consequently, the influence of the low-energy trap states is more significant at 77 K (see previous section). Assuming that both blue and green compartments participate in trapping, the efficiency of trapping with a dissipative rate of $(2500\ ps)^{-1}$ is ~88% while a dissipative rate of $(970\ ps)^{-1}$ yields an efficiency of ~70% (see Figs. 4B and S6 for the kinetics of each compartment). The target analysis of the 45 °C results (see Figs. S7–9 for details) yields efficiencies of ~83% (dissipative rate is $(2500\ ps)^{-1}$) and ~65% (dissipative rate is $(1200\ ps)^{-1}$). To calculate the trapping efficiency without using a specific target model, we used in the next section global analysis of 20 °C, 45 °C and 77 K time-resolved measurements (see Figs. 1 and S7).

3.4. Charge separation and trapping efficiency at 20 °C, 45 °C, and 77 K

The quantum efficiency of photochemistry (i.e. the number of absorbed photons being transferred to the RC and leading to charge separation) in the studied cells of *C. tepidum* is estimated by the following equation, which applies the same concept as used in [25], the formula is:

$$\Phi_{CS} = \frac{DAS_{trap\ 1}}{DAS_{trap\ 1} + DAS_{trap\ 2}}\left(1 - \frac{k_{diss}}{k_{trap1} + k_{diss}}\right) + \frac{DAS_{trap\ 2}}{DAS_{trap\ 1} + DAS_{trapping\ 2}}\left(1 - \frac{k_{diss}}{k_{trap2} + k_{diss}}\right) \quad \text{(See SI for details),}$$

where k_{diss} is the dissipation rate of excitation energy and k_{trap1} is the trapping rate. The total rate of observed fluorescence decay is $k_{trap1} + k_{diss}$. $DAS_{trap\ 1}$ and $DAS_{trap\ 2}$ are the areas under the corresponding DAS that represent trapping. For example, at 20 °C we consider the $(194\ ps)^{-1}$ and $(970\ ps)^{-1}$ DAS (see Fig. 1A) to be due to trapping. Thus, we have $k_{trap1} + k_{diss} = (194\ ps)^{-1}$, $k_{trap2} + k_{diss} = (970\ ps)^{-1}$. $DAS_{trap\ 1}$ and $DAS_{trap\ 2}$ are the areas under the $(194\ ps)^{-1}$ and $(970\ ps)^{-1}$, respectively. We make use of an earlier finding that the efficiency of BChl *c*-to-BChl *a* EET is ~100%. [50]. We consider only the situation that excitations arrive to the reduced RC, in other words, the light intensity should be low enough to ensure that the excitation flow in the photosynthetic apparatus is slower than the turnover of the RC. At higher light intensities, the excitation may arrive to the RC in its oxidized state. In such a case the excitation will be quenched with approximately the same rate constant, but the process will not lead to charge separation (this is an assumption that is based on the analogy between the reaction center of green sulfur bacteria and of photosystem I [40]). We take the intrinsic lifetime of fluorescence, which is 2.5 ns, as the inverse dissipative rate [20].

Table 1 shows a summary of the trapping efficiency calculated in this study. The trapping efficiency at 77 K, 20 °C, and 45 °C is, 81%, 87%, and 83%, respectively. If we take the intrinsic fluorescence lifetime to be 2000 ps instead of 2500 ps then the trapping efficiency at 77 K is calculated to be 76% which is even more in agreement with the efficiency calculated in [11]. These results strongly suggest that the trapping efficiencies at 77 K, 20 °C, and 45 °C do not differ considerably. However, as is obvious from the global analysis, the overall trapping time gets significantly shorter at 20 °C and 45 °C (see Fig. S10). The efficiency at 77 K is not affected much because the trapping rate of $(859\ ps)^{-1}$ is still three times faster than the dissipation rate of $(2500\ ps)^{-1}$.

3.5. Light harvesting in green bacteria at low-light conditions

In a previous study on EET in whole cells of *C. tepidum*, it was shown that the bottleneck of EET is the transfer between the different types of complexes forming the LH apparatus [11]. Therefore it might seem surprising that this low-light adapted bacterium employs three LH complexes containing BChl *a* (baseplate, FMO complexes and core antenna), especially if their spectra are highly overlapping. Such an organization does not seem to have any advantage from an energetic point of view, and must be necessary for another reason. The main function of the FMO complexes is probably to serve as spacers between the chlorosome and the cytoplasmic membrane to allow access of ferredoxin to the RC and at the same time to ensure excitation flow between the chlorosome baseplate and the RC in the cytoplasmic membrane [12,51]. It has been argued before that the baseplate in a chlorosome substantially improves the photosynthetic efficiency by funneling excitations to the reaction centers [29]. Our results suggest that green sulfur bacteria have developed a way of minimizing the losses related to EET between the three complexes. The DAS and the target model reported in this work suggest that all BChl *a* molecules (except the low-energy ones) form one functional compartment implying that the overlapping distributions of energy levels in the baseplate, the FMO complexes and the core antenna lead to the formation of a functional "super-complex" of BChl-*a* containing complexes, and to fast equilibration of the excitations over the whole BChl *a* supercomplex. This may prevent the slowdown of EET at the boundaries between the complexes, leading to high efficiency of trapping in the RCs over a wide range of temperatures.

Our work shows that the trapping efficiency at physiological relevant temperatures in whole cells of *C. tepidum* is substantially higher than what was previously reported for isolated membranes [25] and it is also higher than what was obtained for whole cells at 77 K. Our estimated trapping efficiency also includes BChl *c* and unlike [11,25] is not limited to the EET from FMO to RCs. Apparently, *C. tepidum*, which is able to grow in an environment with very low light conditions, has developed an impressively large light-harvesting system to absorb a large fraction of the limited amount of photons that are available. The number of absorbed photons scales with the number of chlorophylls *N* but also the excitation loss increases with the antenna size, leading to a decrease of the quantum efficiency of excitation trapping Φ_{trap}. In the end, it is the product $N \times \Phi_{trap}$ [52] that reflects the overall light-harvesting capacity and with values of $\Phi_{trap} = \sim 0.85$ and *N* being in the order of $\sim 10^5$, this product is impressively high. This becomes especially clear when a comparison is made with the quantum efficiency of photosystem II of green plants where a similar quantum yield of 0.85 is found for a number of chlorophylls *N* that is only equal to 200–250 and increasing the antenna size beyond this number already leads to a drop in the product $N \times \Phi_{trap}$ [52].

Transparency document

The Transparency document associated with this article can be found, in online version.

Table 1
A summary of the calculated trapping efficiencies at different temperatures.

	Efficiencies estimated from global analysis τ_{int} = 2.5 *ns*	Efficiencies estimated from global analysis τ_{int} = 859 ps (77 K), 970 ps (20 °C), 1200 ps (45 °C)	Efficiencies estimated from target analysis τ_{int} = 2.5 *ns*	Efficiencies estimated from target analysis τ_{int} = 859 ps (77 K), 970 ps (20 °C), 1200 ps (45 °C)
77 K	81%	67%	81%	45%
20 °C	87%	75%	88%	69%
45 °C	83%	72%	83%	65%

Acknowledgments

This work was funded by the Netherlands Organization for Scientific Research (NWO) (project number 10TBSC24-3). This project was carried out within the research programme of BioSolar Cells, co-financed by the Dutch Ministry of Economic Affairs, through grant FOM24. We thank Cor Wolfs for his support with lab supplies and Dr. Arjen Bader for his technical support during the time-resolved measurements.

Appendix A. Supplementary data

Supplementary data to this article can be found online at https://doi.org/10.1016/j.bbabio.2018.12.004.

References

[1] J.T. Beatty, J. Overmann, M.T. Lince, et al., An obligately photosynthetic bacterial anaerobe from a deep-sea hydrothermal vent, Proc. Natl. Acad. Sci. U. S. A. 102 (2005) 9306–9310, https://doi.org/10.1073/pnas.0503674102.
[2] A. Ben-Shem, F. Frolow, N. Nelson, Evolution of photosystem I – from symmetry through pseudosymmetry to asymmetry, FEBS Lett. 564 (2004) 274–280, https://doi.org/10.1016/S0014-5793(04)00360-6.
[3] R.E. Blankenship, Molecular Mechanisms of Photosynthesis, Wiley, 2014.
[4] R.E. Blankenship, K. Matsuura, Antenna complexes from green photosynthetic bacteria, in: B.R. Green, W.W. Parson (Eds.), Light-harvesting Antennas in Photosynthesis, Springer, Netherlands, Dordrecht, 2003, pp. 195–217.
[5] T.P. Causgrove, D.C. Brune, R.E. Blankenship, Förster energy transfer in chlorosomes of green photosynthetic bacteria, J. Photochem. Photobiol. B Biol. 15 (1992) 171–179, https://doi.org/10.1016/1011-1344(92)87014-Z.
[6] J. Chmeliov, G. Trinkunas, H. van Amerongen, L. Valkunas, Light harvesting in a fluctuating antenna, J. Am. Chem. Soc. 136 (2014) 8963–8972, https://doi.org/10.1021/ja5027858.
[7] V. Chukhutsina, L. Bersanini, E.-M. Aro, H. van Amerongen, Cyanobacterial light-harvesting phycobilisomes uncouple from photosystem I during dark-to-light transitions, Sci. Rep. 5 (2015) 14193, , https://doi.org/10.1038/srep14193.
[8] R. Croce, H. van Amerongen, Natural strategies for photosynthetic light harvesting, Nat. Chem. Biol. 10 (2014) 492–501.
[9] J. Currie, D.I. Wilson, OPTI: lowering the barrier between open source optimizers and the industrial MATLAB user, Found Comput. Process Oper. 24 (2012) 32.
[10] J. Dostál, T. Mančal, R. Augulis, et al., Two-dimensional electronic spectroscopy reveals ultrafast energy diffusion in chlorosomes, J. Am. Chem. Soc. 134 (2012) 11611–11617, https://doi.org/10.1021/ja3025627.
[11] J. Dostál, J. Pšenčík, D. Zigmantas, In situ mapping of the energy flow through the entire photosynthetic apparatus, Nat. Chem. 8 (2016) 705–710, https://doi.org/10.1038/nchem.2525.
[12] J. Dostál, F. Vácha, J. Pšenčík, D. Zigmantas, 2D electronic spectroscopy reveals excitonic structure in the baseplate of a chlorosome, J. Phys. Chem. Lett. 5 (2014) 1743–1747, https://doi.org/10.1021/jz5005279.
[13] G.S. Engel, T.R. Calhoun, E.L. Read, et al., Evidence for wavelike energy transfer through quantum coherence in photosynthetic systems, Nature 446 (2007) 782.
[14] R.E. Fenna, B.W. Matthews, Chlorophyll arrangement in a bacteriochlorophyll protein from *Chlorobium limicola*, Nature 258 (1975) 573.
[15] Z. Fetisova, A. Freiberg, K. Mauring, et al., Excitation energy transfer in chlorosomes of green bacteria: theoretical and experimental studies, Biophys. J. 71 (1996) 995–1010, https://doi.org/10.1016/S0006-3495(96)79301-3.
[16] C. Francke, S.C.M. Otte, M. Miller, et al., Energy transfer from carotenoid and FMO-protein in subcellular preparations from green sulfur bacteria. Spectroscopic characterization of an FMO-reaction center core complex at low temperature, Photosynth. Res. 50 (1996) 71–77, https://doi.org/10.1007/BF00018222.
[17] R. Frese, U. Oberheide, I. van Stokkum, et al., The organization of bacteriochlorophyll c in chlorosomes from *Chloroflexus aurantiacus* and the structural role of carotenoids and protein, Photosynth. Res. 54 (1997) 115–126, https://doi.org/10.1023/A:1005903613179.
[18] N.-U. Frigaard, A.G.M. Chew, H. Li, et al., *Chlorobium tepidum*: insights into the structure, physiology, and metabolism of a green sulfur bacterium derived from the complete genome sequence, Photosynth. Res. 78 (2003) 93–117, https://doi.org/10.1023/B:PRES.0000004310.96189.b4.
[19] S. Ganapathy, G.T. Oostergetel, P.K. Wawrzyniak, et al., Alternating syn-anti bacteriochlorophylls form concentric helical nanotubes in chlorosomes, Proc. Natl. Acad. Sci. U. S. A. 106 (2009) 8525–8530, https://doi.org/10.1073/pnas.0903534106.
[20] G. He, D.M. Niedzwiedzki, G.S. Orf, et al., Dynamics of energy and electron transfer in the FMO-reaction center core complex from the phototrophic green sulfur bacterium *Chlorobaculum tepidum*, J. Phys. Chem. B 119 (2015) 8321–8329, https://doi.org/10.1021/acs.jpcb.5b04170.
[21] M.F. Hohmann-Marriott, R.E. Blankenship, Variable fluorescence in green sulfur bacteria, Biochim. Biophys. Acta Bioenerg. 1767 (2007) 106–113, https://doi.org/10.1016/j.bbabio.2006.11.011.
[22] N.P.A. Huner, G. Öquist, A. Melis, Photostasis in plants, green algae and cyanobacteria: the role of light harvesting antenna complexes, in: B.R. Green, W.W. Parson (Eds.), Light-harvesting Antennas in Photosynthesis, Springer, Netherlands, Dordrecht, 2003, pp. 401–421.
[23] M.D. Kamen, A.S. Pietro, Primary Processes in Photosynthesis, Elsevier Science, 2013.
[24] Y.-F. Li, W. Zhou, R.E. Blankenship, J.P. Allen, Crystal structure of the bacteriochlorophyll a protein from *Chlorobium tepidum* 11 Edited by R. Huber, J. Mol. Biol. 271 (1997) 456–471, https://doi.org/10.1006/jmbi.1997.1189.
[25] N.C.M. Magdaong, D.M. Niedzwiedzki, R.G. Saer, et al., Excitation energy transfer kinetics and efficiency in phototrophic green sulfur bacteria, Biochim. Biophys. Acta Bioenerg. 1859 (10) (2018) 1180–1190.
[26] N.C.M. Magdaong, R.G. Saer, D.M. Niedzwiedzki, R.E. Blankenship, Ultrafast spectroscopic investigation of energy transfer in site-directed mutants of the Fenna–Matthews–Olson (FMO) antenna complex from *Chlorobaculum tepidum*, J. Phys. Chem. B 121 (2017) 4700–4712, https://doi.org/10.1021/acs.jpcb.7b01270.
[27] A.K. Manske, J. Glaeser, M.M.M. Kuypers, J. Overmann, Physiology and phylogeny of green sulfur bacteria forming a monospecific phototrophic assemblage at a depth of 100 meters in the Black Sea, Appl. Environ. Microbiol. 71 (2005) 8049–8060, https://doi.org/10.1128/AEM.71.12.8049-8060.2005.
[28] J.T. Nielsen, N.V. Kulminskaya, M. Bjerring, et al., In situ high-resolution structure of the baseplate antenna complex in *Chlorobaculum tepidum*, Nat. Commun. 7 (2016) 12454.
[29] G.T. Oostergetel, H. van Amerongen, E.J. Boekema, The chlorosome: a prototype for efficient light harvesting in photosynthesis, Photosynth. Res. 104 (2010) 245–255, https://doi.org/10.1007/s11120-010-9533-0.
[30] G.S. Orf, R.E. Blankenship, Chlorosome antenna complexes from green photosynthetic bacteria, Photosynth. Res. 116 (2013) 315–331, https://doi.org/10.1007/s11120-013-9869-3.
[31] G.S. Orf, D.M. Niedzwiedzki, R.E. Blankenship, Intensity dependence of the excited state lifetimes and triplet conversion yield in the Fenna–Matthews–Olson antenna protein, J. Phys. Chem. B 118 (2014) 2058–2069, https://doi.org/10.1021/jp411020a.
[32] M.Ø. Pedersen, J. Linnanto, N.-U. Frigaard, et al., A model of the protein—pigment baseplate complex in chlorosomes of photosynthetic green bacteria, Photosynth. Res. 104 (2010) 233–243, https://doi.org/10.1007/s11120-009-9519-y.
[33] J. Pšenčík, S.J. Butcher, R. Tuma, Chlorosomes: Structure, function and assembly, in: M.F. Hohmann-Marriott (Ed.), The Structural Basis of Biological Energy Generation, Springer Netherlands, Dordrecht, 2014, pp. 77–109.
[34] J. Pšenčík, Y.-Z. Ma, J.B. Arellano, et al., Excitation energy transfer dynamics and excited-state structure in chlorosomes of *Chlorobium phaeobacteroides*, Biophys. J. 84 (2003) 1161–1179.
[35] J. Pšenčík, T. Mančal, Light harvesting in green bacteria, in: R. Croce, R. van Grondelle, H. van Amerongen, I. van Stokkum (Eds.), Light Harvesting in Photosynthesis, CRC press, Boca Raton, London, New York, 2018, pp. 121–154.
[36] N.H. Reich, W.G.J.H.M. van Sark, W.C. Turkenburg, Charge yield potential of indoor-operated solar cells incorporated into product integrated photovoltaic (PIPV), Renew. Energy 36 (2011) 642–647, https://doi.org/10.1016/j.renene.2010.07.018.
[37] A.V. Ruban, M.P. Johnson, C.D.P. Duffy, Natural light harvesting: principles and environmental trends, Energy Environ. Sci. 4 (2011) 1643–1650, https://doi.org/10.1039/C0EE00578A.
[38] S. Savikhin, H. van Amerongen, S.L. Kwa, et al., Low-temperature energy transfer in LHC-II trimers from the Chl a/b light-harvesting antenna of photosystem II, Biophys. J. 66 (1994) 1597–1603, https://doi.org/10.1016/S0006-3495(94)80951-8.
[39] S. Savikhin, Y. Zhu, R.E. Blankenship, W.S. Struve, Ultrafast energy transfer in chlorosomes from the green photosynthetic bacterium *Chloroflexus aurantiacus*, J. Phys. Chem. 100 (1996) 3320–3322, https://doi.org/10.1021/jp953734k.
[40] E. Schlodder, M. Hussels, M. Çetin, et al., Fluorescence of the various red antenna states in photosystem I complexes from cyanobacteria is affected differently by the redox state of P700, Biochim. Biophys. Acta Bioenerg. 1807 (2011) 1423–1431, https://doi.org/10.1016/j.bbabio.2011.06.018.

[41] A. Somoza Márquez, L. Chen, K. Sun, Y. Zhao, Probing ultrafast excitation energy transfer of the chlorosome with exciton–phonon variational dynamics, Phys. Chem. Chem. Phys. 18 (2016) 20298–20311, https://doi.org/10.1039/C5CP06491K.
[42] E. Thyrhaug, K. Žídek, J. Dostál, et al., Exciton structure and energy transfer in the Fenna–Matthews–Olson complex, J. Phys. Chem. Lett. 7 (2016) 1653–1660, https://doi.org/10.1021/acs.jpclett.6b00534.
[43] L. Tian, M. Gwizdala, I.H.M. van Stokkum, et al., Picosecond kinetics of light harvesting and photoprotective quenching in wild-type and mutant phycobilisomes isolated from the cyanobacterium *Synechocystis* PCC 6803, Biophys. J. 102 (2012) 1692–1700, https://doi.org/10.1016/j.bpj.2012.03.008.
[44] L. Tian, I.H.M. Van Stokkum, R.B.M. Koehorst, et al., Site, rate, and mechanism of photoprotective quenching in cyanobacteria, J. Am. Chem. Soc. 133 (2011) 18304–18311, https://doi.org/10.1021/ja206414m.
[45] H.-W. Trissl, Modeling the excitation energy capture in thylakoid membranes, in: A.W.D. Larkum, S.E. Douglas, J.A. Raven (Eds.), Photosynthesis in Algae, Springer, Netherlands, Dordrecht, 2003, pp. 245–276.
[46] D.E. Tronrud, J. Wen, L. Gay, R.E. Blankenship, The structural basis for the difference in absorbance spectra for the FMO antenna protein from various green sulfur bacteria, Photosynth. Res. 100 (2009) 79–87, https://doi.org/10.1007/s11120-009-9430-6.
[47] P.I. van Noort, Y. Zhu, R. Lobrutto, R.E. Blankenship, Redox effects on the excited-state lifetime in chlorosomes and bacteriochlorophyll c oligomers, Biophys. J. 72 (1997) 316–325, https://doi.org/10.1016/S0006-3495(97)78670-3.
[48] I.H.M. van Stokkum, B. van Oort, F. van Mourik, et al., (Sub)-picosecond spectral evolution of fluorescence studied with a synchroscan streak-camera system and target analysis, in: T.J. Aartsma, J. Matysik (Eds.), Biophysical Techniques in Photosynthesis, Springer, Netherlands, Dordrecht, 2008, pp. 223–240.
[49] S.I.E. Vulto, M.A. de Baat, S. Neerken, et al., Excited state dynamics in FMO antenna complexes from photosynthetic green sulfur bacteria: a kinetic model, J. Phys. Chem. B 103 (1999) 8153–8161, https://doi.org/10.1021/jp984702a.
[50] J. Wang, D.C. Brune, R.E. Blankenship, Effects of oxidants and reductants on the efficiency of excitation transfer in green photosynthetic bacteria, Biochim. Biophys. Acta Bioenerg. 1015 (1990) 457–463, https://doi.org/10.1016/0005-2728(90)90079-J.
[51] J. Wen, H. Zhang, M.L. Gross, R.E. Blankenship, Membrane orientation of the FMO antenna protein from *Chlorobaculum tepidum* as determined by mass spectrometry-based footprinting, Proc. Natl. Acad. Sci. 106 (2009) 6134–6139, https://doi.org/10.1073/pnas.0901691106.
[52] E. Wientjes, H. van Amerongen, R. Croce, Quantum yield of charge separation in photosystem II: functional effect of changes in the antenna size upon light acclimation, J. Phys. Chem. B 117 (2013) 11200–11208, https://doi.org/10.1021/jp401663w.
[53] C.A. Wraight, R.K. Clayton, The absolute quantum efficiency of bacteriochlorophyll photooxidation in reaction centres of *Rhodopseudomonas spheroides*, Biochim. Biophys. Acta Bioenerg. 333 (1974) 246–260, https://doi.org/10.1016/0005-2728(74)90009-7.